Engineering 6 (2020) 913–918

Contents lists available at ScienceDirect

Engineering

journal homepage: www.elsevier.com/locate/eng

Research
Geodesy and Survey Engineering—Article

Analysis of the Quality of Daily DEM Generation with Geosynchronous InSAR

Zefa Yang [a,b], Qingjun Zhang [c], Xiaoli Ding [b,*], Wu Chen [b]

[a] School of Geosciences and Info-Physics, Central South University, Changsha 410083, China
[b] Department of Land Surveying and Geo-Informatics, The Hong Kong Polytechnic University, Hong Kong 999077, China
[c] China Aerospace Science and Technology Corporation, Beijing 100048, China

ARTICLE INFO

Article history:
Received 20 October 2018
Revised 28 September 2019
Accepted 29 June 2020
Available online 15 July 2020

Keywords:
Daily digital elevation model
Interferometric synthetic aperture radar
Geosynchronous synthetic aperture radar
Accuracy analysis

ABSTRACT

Up-to-date digital elevation model (DEM) products are essential in many fields such as hazards mitigation and urban management. Airborne and low-earth-orbit (LEO) space-borne interferometric synthetic aperture radar (InSAR) has been proven to be a valuable tool for DEM generation. However, given the limitations of cost and satellite repeat cycles, it is difficult to generate or update DEMs very frequently (e.g., on a daily basis) for a very large area (e.g., continental scale or greater). Geosynchronous synthetic aperture radar (GEOSAR) satellites fly in geostationary earth orbits, allowing them to observe the same ground area with a very short revisit time (daily or shorter). This offers great potential for the daily DEM generation that is desirable yet thus far impossible with space-borne sensors. In this work, we systematically analyze the quality of daily GEOSAR DEM. The results indicate that the accuracy of a daily GEOSAR DEM is generally much lower than what can be achieved with typical LEO synthetic aperture radar (SAR) sensors; therefore, it is important to develop techniques to mitigate the effects of errors in GEOSAR DEM generation.

1. Introduction

Digital elevation models (DEMs) are useful in many practical applications, including civil engineering, hydrology, gravity field modeling, urban planning and management, and emergency response. It is often necessary to rapidly generate and frequently update DEM products to keep them up to date in order to support the various applications. There are many methods for generating DEMs, including traditional geodetic survey approaches (e.g., using total stations and Global Navigation Satellite System (GNSS) equipment), airborne laser imaging, detetion, and ranging (LiDAR), photogrammetry, and interferometric synthetic aperture radar (InSAR). Photogrammetry and InSAR are remote sensing techniques that provide high spatial resolution products at a low cost, in comparison with traditional geodetic approaches. Nowadays, InSAR is often the preferred remote sensing technique for generating large-scale DEMs, given its advantages of weather independence and day and night functionality [1–3].

Despite the advantages of InSAR in DEM generation, it is still very difficult to generate or update DEM products frequently (e.g., on a daily basis) over a very large area (e.g., continental or global) with the existing airborne and/or low-earth-orbit (LEO) space-borne synthetic aperture radar (SAR) sensors. First, it is very costly and time-consuming to generate a high-resolution large-scale DEM with airborne or space shuttle SAR sensors. For example, the Shuttle Radar Topography Mission (SRTM) acquired a nearly global high-resolution (~30 m) DEM (covering about 80% of the earth's land mass) over 11 days (i.e., from 16 to 27 September 1999) with a cost of 220 million USD [2,4]. Due to the limited repeat cycles (generally dozens of days) and small spatial coverage, it is also nearly impossible to achieve daily DEM updates with LEO space-borne SAR interferometry. For example, the German Aerospace Center produced a global DEM using TanDEM-X SAR interferometry [5,6] with data over about four years, from 2010 to 2014.

Geosynchronous SAR (GEOSAR) concepts were originally presented by Tomiyasu and Pacelli [7,8] for observing the earth at a higher frequency. With an altitude of about 36 000 km, GEOSAR sensors can acquire SAR images over a much larger footprint (e.g., 8×10^7 km^2 for ScanSAR mode) and with a high

* Corresponding author.
E-mail address: xl.ding@polyu.edu.hk (X. Ding).

https://doi.org/10.1016/j.eng.2020.07.003

spatial resolution (e.g., several meters) in a very short repeat cycle (e.g., 24 h or even as low as dozens of minutes with a constellation of satellites) [9,10]. Typically, GEOSAR can retrieve full three-dimensional (3D) displacement components with sub-centimeter-level accuracy [10], offering 24 h global hazard monitoring with a constellation consisting of multiple GEOSAR satellites. This topic has been extensively discussed recently [11–14]. In addition, the potential for atmospheric phase screen estimation with GEOSAR data has been discussed [15–17].

A great potential of GEOSAR is its ability to provide a daily DEM update over a large area (e.g., globally). The daily (or shorter) repeat cycle of GEOSAR can provide daily SAR interferometry for global DEM generation (or updating). Furthermore, the short repeat cycle can effectively limit the temporal decorrelation of GEOSAR interferometry [18]. Therefore, a DEM can even be generated for regions covered by dense forest and vegetation. In addition, the GEOSAR system can generally allow much larger critical baselines (e.g., up to several hundreds of kilometers) than LEO SAR systems (generally several kilometers) [19]. This means that most GEOSAR data can be used for DEM generation.

In this work, we will systematically analyze the potential of GEOSAR for daily global DEM generation or updating, with a particular focus on the quality of such DEM products. An overview of InSAR-based DEM generation will be presented first. The main error sources and limitations of GEOSAR InSAR and its influences on GEOSAR-based DEM estimation will then be analyzed.

2. InSAR-based DEM generation

Height information of the earth's surface can be estimated from the interferometric phase of InSAR [19]. Fig. 1 depicts the observational geometry of a repeated InSAR system, in which A_1 and A_2 denote the two locations of the SAR antennas with a spatial baseline of B; α is the baseline inclination angle with respect to the horizontal direction; H and θ are the altitude and look angle of the SAR antenna A_1; ρ and $\rho+\Delta\rho$ are the ranges between the SAR antennas A_1 and A_2 with the same ground target; and $Z(y)$ denotes the surface elevation. It can be found from Fig. 1 that [20]

$$Z(y) = H - \rho\cos\theta \tag{1}$$

$$\sin(\alpha-\theta) = \frac{(\rho+\Delta\rho)^2 - \rho^2 - B^2}{2\rho B} \tag{2}$$

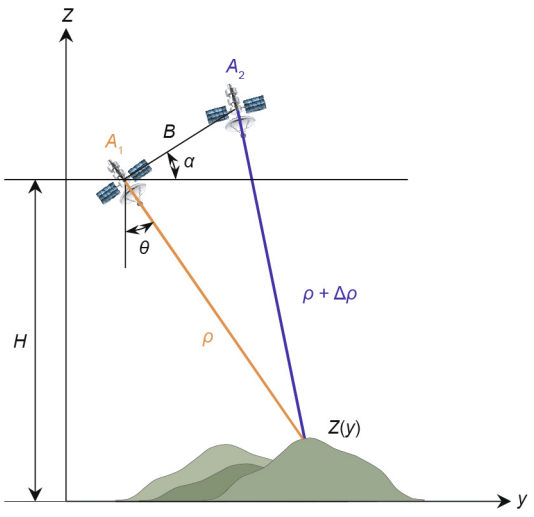

Fig. 1. 2D observational geometry of InSAR for DEM generation.

Let φ be the unwrapped phase difference between antennas A_1 and A_2, that is, the slant-range difference $\Delta\rho$ between the antennas and the same ground target:

$$\Delta\rho = \frac{\lambda\varphi}{4\pi} \tag{3}$$

By combining Eqs. (1)–(3), the relationship between the interferometric phase φ and the surface elevation $Z(y)$ can be obtained:

$$Z(y) = H - \frac{\left(\frac{\lambda\varphi}{4\pi}\right)^2 - B^2}{2B\sin(\alpha-\theta) - \frac{\lambda\varphi}{2\pi}}\cos\theta \tag{4}$$

3. Analysis of error in GEOSAR DEM generation

As observed in Eq. (4), the elevation $Z(y)$ is related to several parameters, including the satellite altitude H, slant-range ρ, look angle θ, wavelength λ, spatial baseline B, inclination angle α, and interferometric phase φ. Some parameters (e.g., wavelength λ) can be accurately determined and considered as error-free, while other parameters such as slant-range, spatial baseline, inclination angle, satellite altitude difference, and interferometric phase may contain errors. In this section, we will analyze the effects of these errors on GEOSAR DEM generation based on the system parameters used in Ref. [10] (see Table 1).

3.1. Slant-range error

Assuming that the error sources are independent of each other, the effect of the slant-range error δ_ρ on InSAR-based DEM estimates δ_Z can be expressed according to Eq. (1):

$$\delta_Z = \cos\theta\cdot\delta_\rho \tag{5}$$

Fig. 2 shows the uncertainties in GEOSAR DEM generation due to slant-range errors as calculated by Eq. (5). Note that a nominal look angle (i.e., 4.8°) was used in this study for simplicity. It can be seen from the results that the slant-range error is linearly propagated into the DEM estimates. Considering that the slant-range error (which is mainly due to tropospheric and ionospheric delays) may be up to dozens of or even hundreds of meters, its influence on DEM estimates is very significant and should be mitigated as much as possible. This issue will be discussed again in detail in Section 4.3.

3.2. Spatial baseline error

According to Eq. (3), the effect of the spatial baseline error δ_B on GEOSAR DEM generation is

$$\delta_Z \approx \frac{\rho\sin\theta\tan(\theta-\alpha)}{B}\cdot\delta_B \tag{6}$$

As seen from Eq. (6), propagation of the spatial baseline error primarily depends on the slant range ρ, look angle θ, baseline inclination angle α, and spatial baseline B. The slant range and look

Table 1
Parameters of the GEOSAR system adopted in the analysis.

Parameter	Values
Altitude	35 788 km
Inclination	60°
Repeat cycle	1 day
Look angle	±1.6°–8.0° (4.8° nominal)
Ground incidence angle	±10.6°–66.4° (38.5° nominal)
Wavelength	24 cm (L-band)
Ground range resolution	20 m nominal
Subswath width	400 km nominal

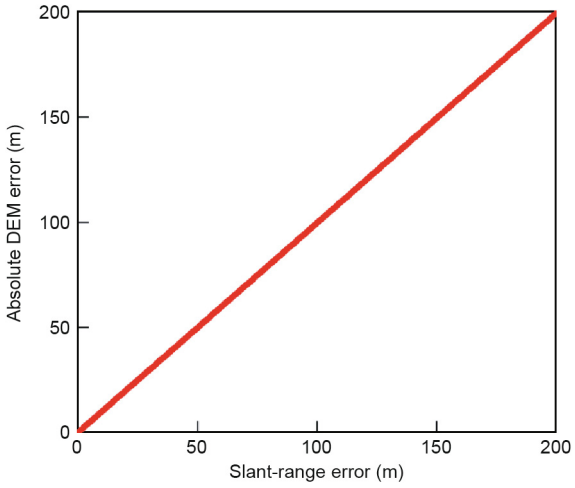

Fig. 2. Absolute DEM errors with respect to slant-range errors with a nominal look angle of 4.8°.

angle are fixed once the imaging geometry is known. Hence, the propagation of the baseline error primarily depends on the spatial baseline and the inclination angle.

Fig. 3 shows the DEM errors due to baseline errors with respect to different spatial baselines (i.e., 0–200 km) and baseline inclination angles (i.e., 0°, ±30°, ±60°, and ±90°). The results indicate that the spatial baselines and baseline inclination angles significantly affect the results. For the same baseline error, the larger the spatial baseline, the smaller the DEM errors will be, and vice versa. On the other hand, for the same baseline error, the larger the inclination angle, the smaller the DEM errors will become, and vice versa. This means that keeping a small inclination angle can improve the accuracy of DEM estimates. The results also suggest that baseline errors are a major error source in GEOSAR DEM generation, especially for small baselines and baselines with large inclination angles.

3.3. Baseline inclination angle errors

Based on Eqs. (1) and (2), the effect of the baseline inclination angle error δ_α on the GEOSAR DEM estimate δ_Z is

$$\delta_Z = \rho \cdot \sin\theta \cdot \delta_\alpha \tag{7}$$

Apparently, the propagation of baseline inclination angle errors depends on the slant range and look angle of the GEOSAR system. Fig. 4 shows DEM errors due to baseline inclination angle errors. The slant range and look angle of the GEOSAR system used are based on those in Table 1. It is seen that the baseline inclination angle error has a great effect on the accuracy of DEM estimates. For example, for a GEOSAR baseline inclination angle error within ±0.01° (three times the standard deviation), the maximum DEM error can be up to about 524 m. Even though one standard deviation (about ±0.0033°) of the baseline inclination angle is considered, the maximum DEM error can be up to 173 m. The results indicate that the inclination angle errors are a significant error source in GEOSAR-based DEM generation.

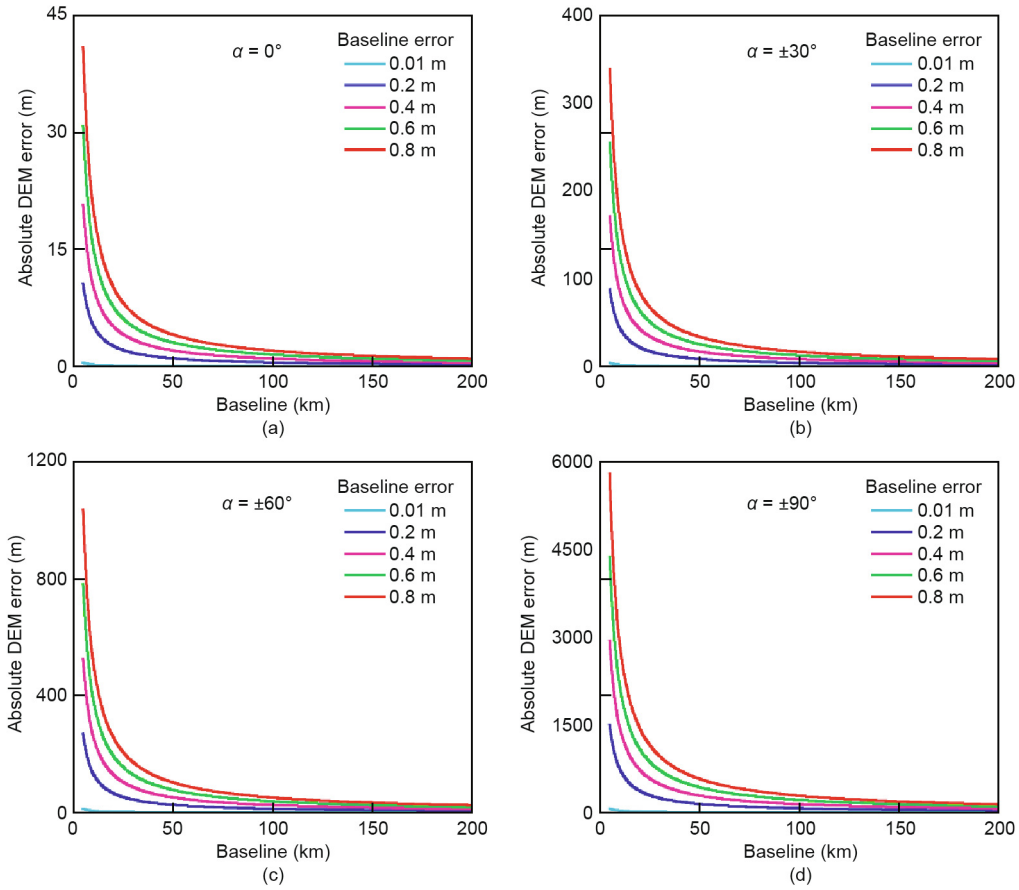

Fig. 3. Absolute DEM errors due to baseline errors with respect to different spatial baselines and baseline inclination angles (i.e., 0°, ±30°, ±60°, and ±90° for (a)–(d)). A nominal look angle of 4.8° is used.

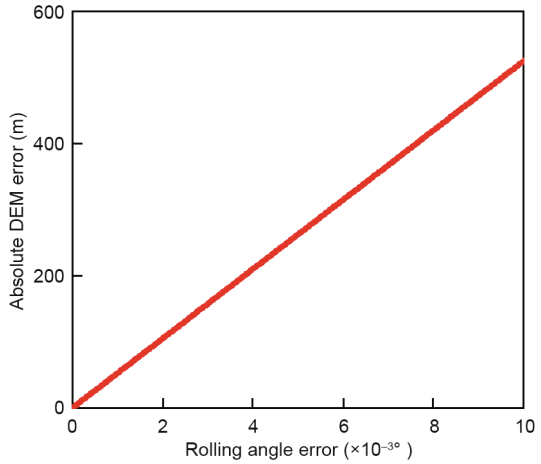

Fig. 4. Absolute DEM errors due to baseline angle inclination errors. A nominal look angle of 4.8° is used.

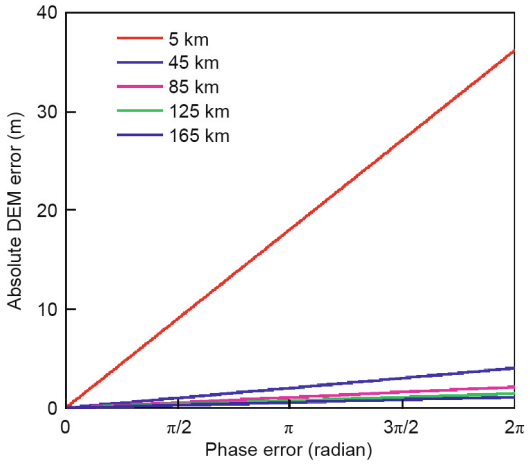

Fig. 5. Absolute DEM errors due to interferometric phase errors with respect to different spatial baselines (i.e., 5, 45, 85, 125, and 165 km) with $\theta = 4.8^\circ$ (nominal) and $\alpha = 0^\circ$.

3.4. Satellite altitude errors

From Eq. (1), the DEM error δ_Z due to the errors in satellite altitude δ_H can be expressed as follows:

$$\delta_Z = \delta_H \tag{8}$$

Considering that the accuracy level of satellite altitude determination is generally at the centimeter to meter level, the effect of GEOSAR altitude errors is insignificant compared with the other error sources.

3.5. Interferometric phase errors

According to Eq. (4), the effect of the interferometric phase error δ_φ on the DEM error δ_Z can be described as follows:

$$\delta_Z = \frac{\lambda\rho}{4\pi B}\frac{\sin\theta}{\cos(\theta-\alpha)}\delta_\varphi \tag{9}$$

Fig. 5 plots the DEM errors due to interferometric phase errors. Phase errors can significantly affect the accuracy of GEOSAR DEM, especially in the case of small spatial baselines. For example, a phase error of 2π gives results with about 36 m DEM error for a baseline of 5 km, while the DEM error is reduced to about 4 m when the baseline increases to 45 km (see Fig. 5).

4. Quality of daily GEOSAR global DEM

As stated earlier, a GEOSAR system has the potential to generate a daily global DEM, due to the very short satellite revisit time and very large spatial coverage. However, the quality of such a DEM may be limited by intrinsic error sources such as ① those analyzed above, ② dense interferometric phase fringes, and ③ spatial–temporal variation of the atmospheric conditions.

4.1. Influence of intrinsic error sources

As analyzed in Section 3, five major intrinsic error sources (i.e., slant-range errors, satellite altitude errors, spatial baseline errors, baseline inclination angle errors, and phase errors) can affect the accuracy of GEOSAR DEM generation. These errors affect DEM generation with either GEOSAR or LEO SAR sensors. However, due to the much higher altitude of GEOSAR satellites (about 36 000 km), the impacts of these errors often become much more significant (up to around 50 times greater than those in SAR DEM generation with LEO sensors). As a result, the accuracy of GEOSAR DEM can be much lower than the DEM generated from LEO SAR sensors, if the errors cannot be mitigated properly.

Various methods have been developed for improving the accuracy of InSAR-derived DEM, such as the use of ground control points (corner reflectors) for reducing systematic errors (e.g., baseline and inclination angle errors [21]), multi-baseline InSAR DEM reconstruction for mitigating slant-range errors [3], and maximum *a posteriori* estimation for noise reduction [22]. These methods can potentially be applied to improve the accuracy of GEOSAR DEM, although further research is still required to test these methods and develop new approaches.

4.2. Dense interferometric phase fringes

As discussed in Section 3, the effects of some error sources (i.e., spatial baseline errors and phase errors) on GEOSAR DEM are inversely proportional to the spatial baselines. This means that it is feasible to reduce the effects of these error sources by increasing the spatial baselines. However, longer spatial baselines lead to denser interferometric fringes, as the height ambiguity (Z_{amb}) decreases with the baseline [1]:

$$Z_{\text{amb}} = \frac{\lambda\rho\sin\theta}{2B\cos(\theta-\alpha)} \tag{10}$$

Dense interferometric fringes may give rise to difficulties in phase unwrapping [23]. If the topographic phase cannot be accurately recovered in phase unwrapping, the height of the ground surface cannot be reliably estimated.

To illustrate this issue, simulated interferometric fringes with respect to different spatial baselines are presented in Fig. 6 based on a real DEM (shown in Fig. 6(a)). The elevation varies from 225 to 2160 m. For a spatial baseline of 10 km, the interferometric phase fringes (wrapped) due to surface terrain (see Fig. 6(c)) are acceptable for phase unwrapping. However, when the spatial baseline increases to 50 or 100 km (see Figs. 6(c) and (d)), the topographic phase fringes are too dense to be unwrapped.

There are approaches to overcome this difficulty. For example, an external DEM (e.g., SRTM DEM) may be applied to simulate and remove the main topographic patterns, and phase unwrapping can then be carried out based on the residual topographic phase [24]. Such strategies may need further investigation when used for GEOSAR DEM generation.

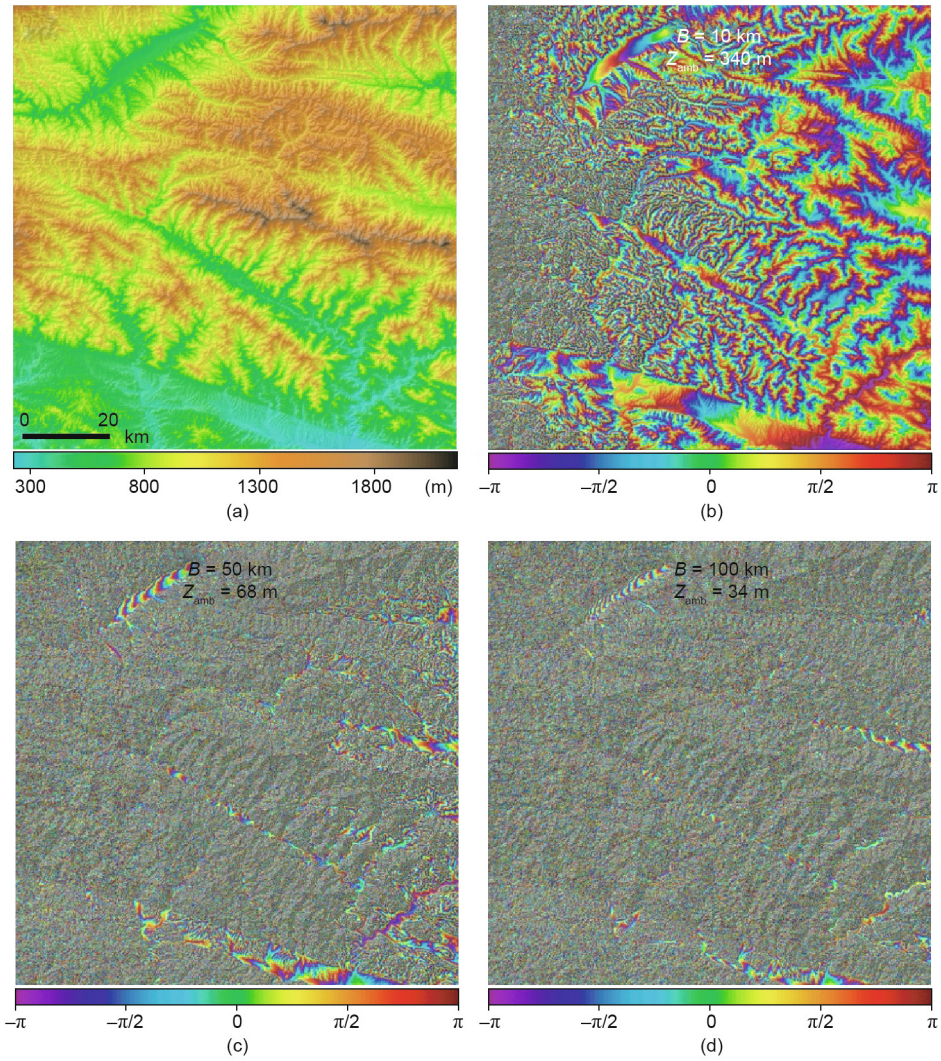

Fig. 6. (a) A DEM; (b)–(d) wrapped interferometric topographic phase for spatial baselines of 10, 50, and 100 km, respectively.

4.3. Effect of temporal-spatial variation of the atmosphere

GEOSAR signals propagate through the full atmosphere (including the troposphere and ionosphere), rather than through only a part of the ionosphere, as is the case for a LEO SAR sensor. Moreover, a GEOSAR has a much longer integration time (from hundreds to thousands of seconds) than a LEO SAR (from several to dozens of seconds) [25]. The atmospheric conditions vary both in time and space, and may cause significant errors in InSAR products [26,27]. Therefore, methods should be developed to better mitigate atmospheric effects (e.g., Refs. [28–30]) to improve the accuracy of GEOSAR daily DEM products.

5. Conclusions

GEOSAR satellites offer the potential for daily DEM generation due to the very short satellite revisit time and the very large footprint of GEOSAR. We have analyzed the potential quality of such DEMs and found that, due to the very high altitude of GEOSAR satellites, the accuracy level of a GEOSAR DEM may be much lower than that from typical LEO SAR sensors. Therefore, strategies should be developed to better mitigate the error sources of a GEOSAR DEM.

Acknowledgements

This work was partly supported by the Research Grants Council (RGC) of Hong Kong Special Administrative Region (PolyU 152232/17E and PolyU 152164/18E), Research Institute for Sustainable Urban Development of the Hong Kong Polytechnic University (1-BBWB).

Compliance with ethics guidelines

Zefa Yang, Qingjun Zhang, Xiaoli Ding, and Wu Chen declare that they have no conflict of interest or financial conflicts to disclose.

References

[1] Hanssen RF. Radar interferometry: data interpretation and error analysis. New York: Kluwer Academic Publishers; 2001.
[2] Farr TG, Rosen PA, Caro E, Crippen R, Duren R, Hensley S, et al. The shuttle radar topography mission. Rev Geophys 2007;45(2):RG2004.
[3] Ferretti A, Prati C, Rocca F. Multibaseline InSAR DEM reconstruction: the wavelet approach. IEEE Trans Geosci Remote Sens 1999;37(2):705–15.
[4] Rabus B, Eineder M, Roth A, Bamler R. The shuttle radar topography mission—a new class of digital elevation models acquired by spaceborne radar. ISPRS J Photogramm Remote Sens 2003;57(4):241–62.

[5] Gruber A, Wessel B, Huber M, Roth A. Operational TanDEM-X DEM calibration and first validation results. ISPRS J Photogramm Remote Sens 2012;73:39–49.
[6] Rizzoli P, Martone M, Gonzalez C, Wecklich C, Borla Tridon D, Bräutigam B, et al. Generation and performance assessment of the global TanDEM-X digital elevation model. ISPRS J Photogramm Remote Sens 2017;132:119–39.
[7] Tomiyasu K, Pacelli JL. Synthetic aperture radar imaging from an inclined geosynchronous orbit. IEEE Trans Geosci Remote Sens 1983;GE-21(3):324–9.
[8] Tomiyasu K. Synthetic aperture radar in geosynchronous orbit. In: Proceedings of the 1978 Antennas and Propagation Society International Symposium; 1978 Mar 15–19; Washington, DC, USA; 1978.
[9] Guarnieri AM, Tebaldini S, Rocca F, Broquetas A. GEMINI: geosynchronous SAR for earth monitoring by interferometry and imaging. In: Proceedings of the 2012 IEEE International Geoscience and Remote Sensing Symposium; 2012 Jul 22–27; Munich, Germany; 2012.
[10] Chao B, Harding D, Cohen S, Luthcke S, Hofton M, Blair JB. Global Earthquake Satellite System requirements derived from a suite of scientific observational and modeling studies. Final Reports. Washington, DC: National Aeronautics and Space Administration; 2002.
[11] Hu C, Li Y, Dong X, Wang R, Cui C. Optimal 3D deformation measuring in inclined geosynchronous orbit SAR differential interferometry. Sci China Inf Sci 2017;60(6):060303.
[12] Zheng W, Hu J, Zhang W, Yang C, Li Z, Zhu J. Potential of geosynchronous SAR interferometric measurements in estimating three-dimensional surface displacements. Sci China Inf Sci 2017;60(6):060304.
[13] Hu C, Li Y, Dong X, Wang R, Cui C, Zhang B. Three-dimensional deformation retrieval in geosynchronous SAR by multiple-aperture interferometry processing: theory and performance analysis. IEEE Trans Geosci Remote Sens 2017;55(11):6150–69.
[14] Kou L, Wang X, Xiang M, Zhu M. Interferometric estimation of three-dimensional surface deformation using geosynchronous circular SAR. IEEE Trans Aerosp Electron Syst 2012;48(2):1619–35.
[15] Ruiz-Rodon J, Broquetas A, Makhoul E, Monti Guarnieri A, Rocca F. Nearly zero inclination geosynchronous SAR mission analysis with long integration time for earth observation. IEEE Trans Geosci Remote Sens 2014;52(10):6379–91.
[16] Li D, Rodriguez-Cassola M, Prats-Iraola P, Dong Z, Wu M, Moreira A. Modelling of tropospheric delays in geosynchronous synthetic aperture radar. Sci China Inf Sci 2017;60(6):060307.
[17] Ji Y, Zhang Q, Zhang Y, Dong Z. L-band geosynchronous SAR imaging degradations imposed by ionospheric irregularities. Sci China Inf Sci 2017;60(6):060308.
[18] Zebker HA, Villasenor J. Decorrelation in interferometric radar echoes. IEEE Trans Geosci Remote Sens 1992;30(5):950–9.
[19] Bamler R, Hartl P. Synthetic aperture radar interferometry. Inverse Probl 1998;14(4):R1–R54.
[20] Zebker HA, Goldstein RM. Topographic mapping from interferometric synthetic aperture radar observations. J Geophys Res Solid Earth 1986;91(B5):4993–9.
[21] Rufino G, Moccia A, Esposito S. DEM generation by means of ERS tandem data. IEEE Trans Geosci Remote Sens 1998;36(6):1905–12.
[22] Ferraiuolo G, Pascazio V, Schirinzi G. Maximum *a posteriori* estimation of height profiles in InSAR imaging. IEEE Geosci Remote Sens Lett 2004;1(2):66–70.
[23] Chen CW, Zebker HA. Two-dimensional phase unwrapping with use of statistical models for cost functions in nonlinear optimization. J Opt Soc Am A 2001;18(2):338–51.
[24] Zhou C, Ge L, Dong C, Chang H. A case study of using external DEM in InSAR DEM generation. Geo Spat Inf Sci 2005;8(1):14–8.
[25] Long T, Hu C, Ding Z, Dong X, Tian W, Zeng T. Geosynchronous SAR: system and signal processing. Singapore: Springer Nature Singapore Pte Ltd.; 2018.
[26] Ishimaru A, Kuga Y, Liu J, Kim Y, Freeman T. Ionospheric effects on synthetic aperture radar at 100 MHz to 2 GHz. Radio Sci 1999;34(1):257–68.
[27] Sun J, Bi Y, Wang Y, Hong W. High resolution SAR performance limitation by the change of tropospheric refractivity. In: Proceedings of 2011 IEEE CIE International Conference on Radar; 2011 Oct 24–27; Chengdu; 2011.
[28] Hu C, Li Y, Dong X, Wang R, Ao D. Performance analysis of L-band geosynchronous SAR imaging in the presence of ionospheric scintillation. IEEE Trans Geosci Remote Sens 2017;55(1):159–72.
[29] Meyer FJ. Performance requirements for ionospheric correction of low-frequency SAR data. IEEE Trans Geosci Remote Sens 2011;49(10):3694–702.
[30] Tian Y, Hu C, Dong X, Zeng T, Long T, Lin K, et al. Theoretical analysis and verification of time variation of background ionosphere on geosynchronous SAR imaging. IEEE Geosci Remote Sens Lett 2015;12(4):721–5.